

Title:

**Terahertz radiation generation by three-color laser pulses in air filament**

Authors:

V. Vaičaitis, O. Balachninaitė, U. Morgner and I. Babushkin

**Manuscript**

The original publication may be found at:

Journal: Journal of Applied Physics 125, 173103 (2019)

DOI: <https://doi.org/10.1063/1.5078683>

# Terahertz radiation generation by three-color laser pulses in air filament

V. Vaičaitis<sup>1,a)</sup>, O. Balachninaite<sup>1</sup>,  
U. Morgner<sup>2,3</sup>, I. Babushkin<sup>2,3,4</sup>

<sup>1</sup>Laser Research Center, Vilnius University, Saulėtekio 10, Vilnius LT-10223, Lithuania.

<sup>2</sup>Institute of Quantum Optics, Leibniz University of Hannover, D30167 Germany.

<sup>3</sup>Cluster of Excellence PhoenixD (Photonics, Optics, and Engineering – Innovation Across Disciplines), D30167 Germany.

<sup>4</sup>Max Born Institute, Berlin, D10117 Germany.

a) Electronic mail: Virgilijus.Vaicaitis@ff.vu.lt

We demonstrated terahertz (THz) radiation generated from a three-color laser-excited filament in air for a wide tuning range and various wavelength ratios of the pump laser pulses. As a pump source the radiation of the femtosecond Ti:sapphire laser and infrared output of the optical parametric generator were used. It was found that the spectrum of generated THz pulses spans up to 50 THz, while the overall THz generation efficiency is of an order of magnitude larger than the one produced by two color pulses in an analogous configuration. Our results support the idea that three-color pulses are more suitable for broadband THz generation, since the corresponding waveforms can produce faster free electrons in larger quantities. We have found that the conversion efficiency is significantly limited due to intensity clamping. The spectral broadening of THz radiation is explained by aperiodicity of ionization events in time.

## 1. Introduction

Terahertz (THz) radiation generation from laser-created gas plasma produced by bichromatic femtosecond laser pulses is a simple, efficient, and well-established technique [1–3]. Though, by using the Ti:Sapphire laser pulses as a pump source, this method of THz generation allows to obtain very high THz field strengths and extremely broadband spectral widths, generation efficiency still remains quite low and usually does not exceed  $10^{-4}$  [4–7]. In typical experiments, a small plasma spot is induced by strong bichromatic pulses at 800 and 400 nm -- a configuration which is fairly simple and thus attractive.

It is worth to note that the plasma itself can serve as a THz wave sensor [8–11], so the same gas can be used for both the generation and detection of THz radiation. In a promising technique, based on this effect and termed THz air biased coherent detection (THz-ABCD) [8, 9, 12] one can provide the high detection sensitivity and frequency resolution within a wide spectral bandwidth (at least from 0.1 to 40 THz [3]). In this technique, the THz field induces the second harmonics of the optical pump [13].

In order to enhance THz generation efficiency it was proposed to use the longer wavelength driver pulses [14–16], which later was demonstrated experimentally by using a tunable IR light source [17]. In addition, there were both experimental and theoretical reports [18–20] of THz generation by two-color driver pulses with the shift of one of the frequencies from the exact second harmonic (thus making frequency ratio “optically incommensurate” [21]) which showed the THz frequency shifts and also a spectral broadening [22]. Recently, efficient THz radiation generation has been demonstrated using two-color laser scheme with uncommon frequency ratios (such as 1:4 and 2:3) [23–25]. It was also predicted that if number of frequencies forming the driving waveform is larger than two, THz radiation can be generated much more efficiently [26]. In the particular case of a 3-color pump formed with an optical parametric amplifier (OPA) with the pump at around 800 nm and signal and idler tuned around 1600 nm it was also shown theoretically [20] that not only the THz generation

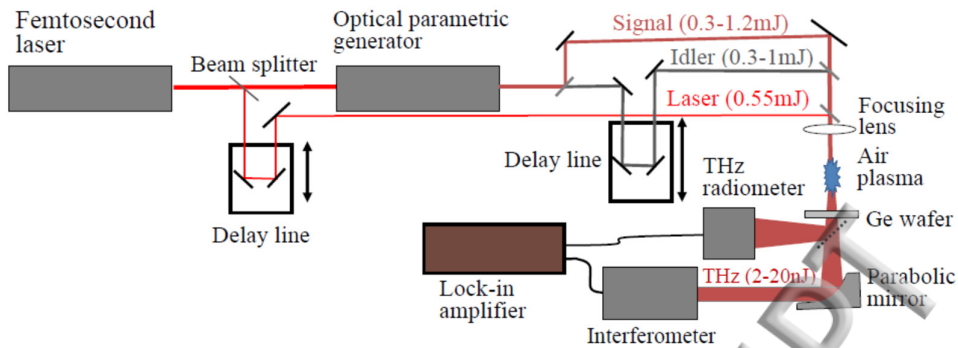


Fig.1. Experimental setup.

efficiency can be enhanced, but also the spectra can be significantly broadened and demonstrate a complicated internal structure.

The 3-color setup provide thus much higher spectral tunability and potentially higher efficiency, and this is a new field of research with only few works existing to date [20,22,27]. In particular, in the experimental studies the absolute generation efficiencies were not yet studied up to now. Besides, the most studies are devoted to the tight focusing, that is, a plasma spot, and not to 3-color pulses in a filament.

If we consider 2-color pulses, it was shown that in contrast to a tight focusing (plasma spot) the filament formation demonstrates richer spatio-temporal dynamics and broader spectra [15,28]. On the other hand, the efficiencies in this case can be somewhat smaller than for the case of plasma spot [29] due to intensity clamping, which however can be compensated or even outperformed by the longer propagation distances [28, 30].

In this paper we extend the 3-color considerations to the realms of filaments. We report the experimental investigation of the energy, spectral and spatial properties of THz radiation generated in air by femtosecond three- and two-color laser filaments of widely tunable wavelengths. We demonstrate the significant spectral broadening of THz spectrum and support the increase of generation efficiency compared to the 2-color pump by an order of magnitude. We support our experimental findings with a simple theoretical model, and explain both the spectral broadening and efficiency increase by the fact that 3-color case provides more suitable waveforms for efficient plasma current generation.

## 2. Experiment

For the experiments we have used a 1 kHz repetition rate femtosecond Ti:sapphire chirped pulse amplification laser system (Legend elite duo HE+, Coherent Inc.), delivering 35-40 fs (FWHM) light pulses centered approximately at 790 nm with maximal pulse energy of 8 mJ. The near-infrared (NIR) laser beam was divided into two beams of unequal intensities by a beam splitter. The more powerful laser pulses (pulse energy of about 7 mJ) was used to pump an optical parametric amplifier (OPA, Light Conversion, Inc.), which produced the tunable infrared (IR) signal and idler wave pulses in the wavelength range between 1.2 and 1.6  $\mu\text{m}$  and between 1.6 and 2.4  $\mu\text{m}$ , respectively (Fig.1).

It is well known that the efficiency of THz radiation generation is most efficient when polarizations of all interacting waves are the same. However, though at the OPA output polarization direction of the signal wave was parallel to that of the laser beam (NIR pump), the polarization of the idler wave was orthogonal to polarizations of the signal and laser beams. Therefore the polarization of the idler wave was rotated by 90 degrees using the broadband metallic mirrors [31].

Since the pulse energy, duration and transverse diameters of the idler and signal beams are strongly dependent on wavelength [32, 33], these parameters were continuously monitored during our experiment. The results are summarized in figures 2 and 3. The durations of the signal and idler

pulses were found to be 43-65 fs and 55-70 fs, respectively. Similarly, the diameters of the signal and idler wave beams have varied between 3.8 and 4.6 and between 2.8 and 3.4 mm, respectively. At the same time the single-pulse energy of the IR pulses has varied between 1.3 and 1.75 mJ (Fig. 3). Note that changes of these laser parameters imply strong pump intensity variations, which consequently may significantly impact THz radiation generation. Therefore these wavelength dependencies were taken into account during theoretical modelling and interpretation of the experimental results.

The IR signal wave pulses were superposed concentrically with the idler and NIR laser pulses with the help of two thin dichroic beam splitters (Fig. 1). The relative temporal delay between the IR signal, idler and NIR laser pulses was controlled by the two motorized and computer-controlled optical delay lines. The IR and NIR laser pulses were temporally overlapped and focused in air by the lens with the focal length of 20 cm and as a result the visible plasma filament of about 1 cm long was produced.

Note that the relative phases of the pump waves were not controlled during the experiment,

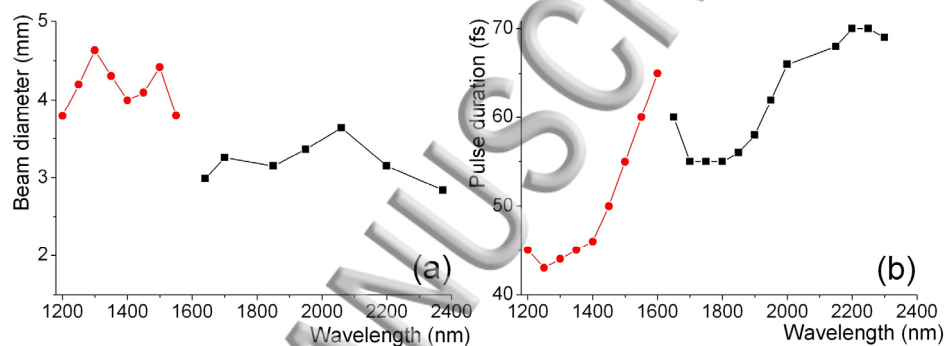


Fig.2. Wavelength dependencies of (a) the beam diameter and (b) pulse durations of the signal (red circles) and idler (black squares) waves of the OPA.

therefore the measurements of THz radiation were averaged over these phases. However, our modelling showed that the result depends very little on these parameters, probably due to the fact that in the case of detuned frequencies the relative phases are strongly varying anyway during pulse propagation through interaction region.

The visible, IR and NIR pump radiations were filtered out by a 2 mm-thick Ge wafer and special long-pass THz filters (LPF23.4, Tydex company). The cut-off frequency of Ge wafer is about 1.9  $\mu\text{m}$  and it is transparent between 1.9 and at least 24  $\mu\text{m}$  (between 12 and 150 THz, respectively). Similarly, the cut-off frequency of the used long-pass THz filters was 13  $\mu\text{m}$  (23 THz) with the transparency range spanning up to 1200  $\mu\text{m}$  (0.25 THz).

As it was mentioned above, the THz-ABCD detection allows spectral characterization of the broadband THz pulses. However, in our experiment we have chosen an interferometric THz pulse characterization, which is more simple and independent on the probe pulse duration [4].

Therefore during spectral measurements THz radiation generated in the filament was collimated by the metal-coated parabolic mirror and directed into a home-made THz Michelson interferometer consisting of a 2 micrometer-thick nitrocellulose beam splitter and two flat metal-coated mirrors. One of these mirrors was placed on a computer-controlled translation stage, therefore by varying its position we were able to record the interference traces of the input THz radiation and receive the spectral information, since the Fourier transform of these temporal traces gives the spectrum of the THz pulses. Importantly, this approach does not need the carrier-envelope offset stabilization of the pulses, in contrast to the electro-optic sampling approach used for instance in [22].

The energy of generated THz pulses was measured using a calibrated pyroelectric detector. Its response function was linear and flat with relative accuracy of better than 20% at least in the range

of 0.1-30 THz. The voltage responsivity of the detector was 63.7 kV/W at 5 Hz repetition rate. Thus, since the laser repetition rate was 1 kHz, 1 mV voltage given by the detector was equivalent to about 15.7  $\mu$ J of single THz pulse energy.

During investigations of the spatial THz beam profile this detector has been placed on the computer-controlled motorized translation stage located at about 50 cm from the plasma filament. Since the dimensions of the THz beam were much larger than the aperture of the detector, by moving it across the THz beam we were able to register the corresponding angular spectra of generated radiation. However, during these measurements only the integrated over available spectral range spatial distribution of THz radiation has been measured.

### 3. Results and discussion

Dependence of THz pulse energy on the three-color pump wavelength is presented in Fig. 3a. Note that the wavelengths of the signal and idler waves are related, since during optical parametric interaction the frequencies of the pump and generated photons must obey the law of energy conservation. Thus, when the signal wavelength is increased, the wavelength of the idler wave of the OPA automatically decreases, i.e., the sum of the frequencies of the signal and idler waves always remains constant and equal to the pump frequency. Therefore when the signal wavelength was tuned from 1200 to 1580 nm, the wavelength of the idler wave decreased from 2319 to 1583 nm, respectively. Within this pump tuning range the efficient THz radiation generation was observed. In general the efficiency of THz generation was nearly proportional to the pump pulse energy (the NIR laser pulse energy was kept constant at about 0.55 mJ during all the experiment) and therefore was minimal at the extremes of the OPA tuning range and reached its maximal values at the signal wavelength of about 1480 nm. The maximal THz pulse energy registered at this point was about 20 nJ, which implies the total energy conversion efficiency of nearly  $10^{-5}$ . Note that during the experiment the pump focusing conditions were not optimized. Theoretical considerations predict that the optimization of the focusing conditions can increase the output up to two orders of magnitude, however this is beyond the scope of this report.

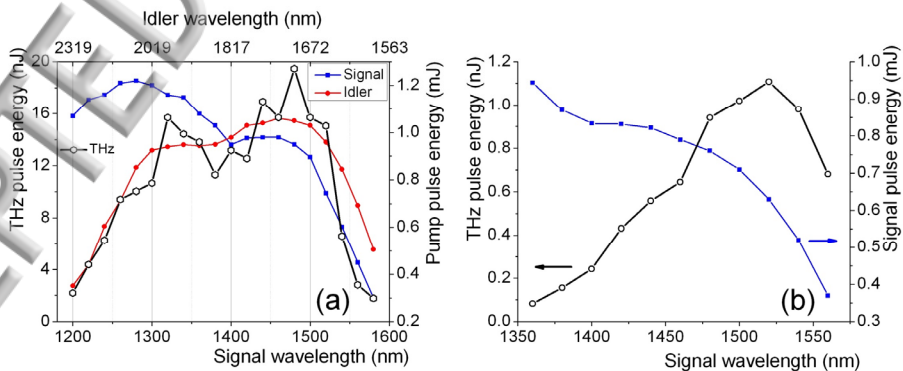


Fig.3. (a) Dependence of THz pulse energy (black line, hollow circles) on the wavelength of signal and idler pulses. Blue and red curves represent the wavelength dependencies of the signal and idler wave pulse energies. (b) Dependence of the THz pulse energy (black line, hollow circles) on the two-colour pump (laser and signal wave pulses) wavelength. The energy of NIR laser pulse was always kept equal to 0.55 mJ.

It is worth to note that much weaker, but still not negligible THz radiation generation was also registered in the case of any two-color pump combination, i. e., when the pulses of the laser and signal wave, laser and idler wave or signal and idler waves were used as the pump source. The most distinct characteristics of THz generation were observed in the case of the laser and signal wave

pump pulses, therefore, below we will refer it as the "two-color pump" or "two-color THz generation". Thus, the dependence of THz pulse energy on the two-color pump wavelength is presented in Fig. 3b. As in the case of three-color pump (Fig.3a), it has maximum at the signal wavelength of about 1500 nm. However, the two-color THz generation efficiency rapidly decreased at shorter signal wave wavelengths, when the pump pulse energy was highest. This result can be explained by the fact that shorter signal wavelengths are more detuned from the NIR laser wavelength and therefore as the signal wavelength decreases, the conditions for THz wave generation become less and less favorable.

Typical interference traces and corresponding power spectra of generated THz radiation are presented in Fig.4. In most cases of the three-color THz generation the non-negligible signal could be observed up to 100 THz. However, the spectrum was highly modulated with the main power located below 50 THz and no clear dependence on the pump wavelength was observed (Fig. 4a). Note that similar spectral modulation was reported in [22], when the tunable incommensurate in wavelength two-color pump pulses were used for the generation of THz radiation.

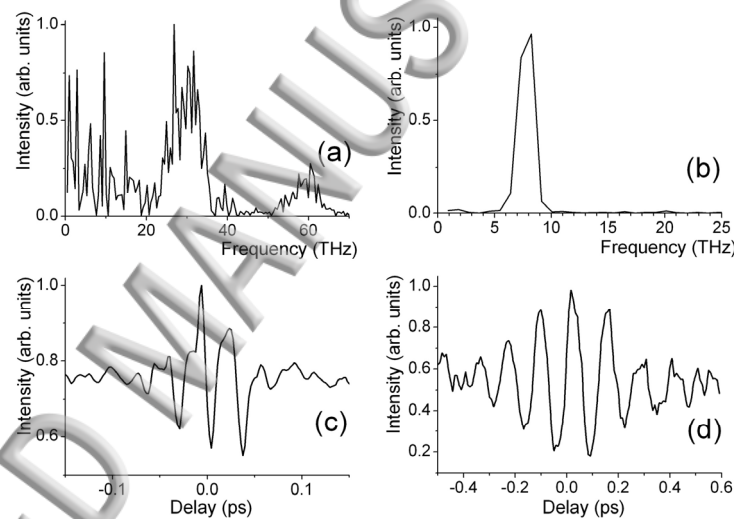


Fig.4. (a, b) Spectra and (c, d) corresponding interference traces of THz radiation generated by (a, c) three-colour and (b, d) two-colour (laser and signal wave) pump. The signal wavelength was 1500 nm in both cases.

In contrast to the three-color pump case the spectrum of THz radiation generated by two-color laser pulse consisted of a very weak broadband background and a single spectral band centered at about 8 THz (FWHM of about 1.8 THz, Fig. 4b). The highest efficiency of THz radiation generation was registered at the signal wavelength of about 1550 nm, a point where the combination of the driver (pump and signal wave) frequencies falls exactly within this spectral THz band. However, the width and central wavelength of this spectral peak was found to be independent on the pump wavelength at least within the signal wave tuning range from 1480 to 1520 nm. This indicates that the narrowband THz generation could be influenced not only by the ionization-induced nonlinearity but also by resonances in excited air molecules. We interpret it in the following way: the spectral broadening of the pump pulses in the air [34,35] may be the reason of the wide signal wave tuning range, while the four-wave mixing (FWM) resonantly enhanced by the THz transitions [36,37] can explain, why the spectral properties of generated narrowband THz radiation were independent on the pump wavelength. In addition, the nonlinear and plasma-related phase shifts of the pump waves

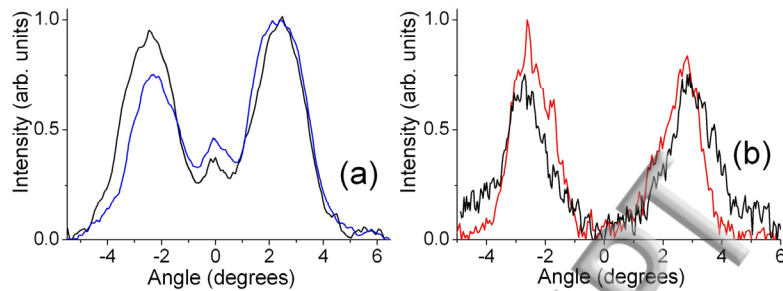


Fig.5. (a) Angular spectra of (a) three-colour THz beam for the signal wavelength of 1400 and 1500 nm (blue and black lines, respectively) and (b) spectra of two-colour THz beam for the signal wavelength of 1500 and 1540 nm (black and red lines, respectively).

[38] also strongly influence the FWM process, including modification of THz radiation generation efficiency and its angular structure.

Intensity dependencies as a function of the propagation angle of THz radiation, generated by the three- and two-color pump, are presented in Fig. 5. Note that these graphs represent only the THz intensity integrated over the whole spectral range (0.1–70 THz, see Fig.4).

Fig. 5 clearly demonstrates the conical nature of the THz beam, which is also characteristic for the THz emission, generated by commensurate two-color laser pulses [39, 40]. However, in contrast to the case of two-color pump, three-color THz beam was not the fully hollow one: along with the off-axis THz radiation the axially directed emission was also registered. Note, that the cone apex angle of the THz beam was about 5 degrees and was nearly independent on the pump wavelength, which is in accord with the models explaining generation of off-axis THz radiation as a result of constructive interference of THz waves emerging from different parts of the pump beam [41, 42].

#### 4. Theoretical consideration

We corroborate our experimental findings with a simple theory which describes the ionization process in a small region of space, that is, neglecting the propagation effects of the driver pulses, such as their spectral, temporal and spatial reshaping. Nevertheless, since we expect that intensity clamping plays the critical role in the dynamics, we take it into account in our model in a simplified way. In our so called local current (LC) model the so called Brunel radiation  $E_{Br}(t)$  is generated by the photoionization-based plasma current  $J(t)$  as  $E_{Br}(t) = g \frac{dJ(t)}{dt}$ , where  $g$  is a geometry-dependent factor [21,22]. The model assumes that the free electrons are born (in process of ionization) with zero velocity. The electron density is given by  $\frac{dp}{dt} = (\rho_0(t) - \rho(t))W(t)$ , where  $\rho_0(t)$  is the density of neutral atoms and  $W(t)$  is the ionization rate. Ionization rate is calculated using static tunnel ionization formula [43]:  $W_{St}(t) = \frac{\alpha}{\tilde{E}(t)} \exp\left\{-\frac{\beta}{\tilde{E}(t)}\right\}$  with  $\tilde{E}(t) = |E(t)|/E_a$ , where  $E_a$  is the atomic unit of field, the coefficients  $\alpha = 4\omega_a r_H^{5/2}$  (here  $\omega_a$  is the atomic unit of frequency) and  $\beta = (2/3)r_H^{3/2}$  are defined through the ratio  $r_H$  of ionization potentials of the molecules under consideration to that of an atomic hydrogen. The way how we use this model (see below) makes the particular value of the ionization potential irrelevant, therefore we assumed argon in our calculations.

We believe that in the experiment the intensity clamping plays a critical role in the pump propagation and ionization dynamics, and therefore in the THz generation. Namely, the peak intensity achieved during the propagation is strongly limited by the ionization. As the intensity achieves the ionization

threshold, a strong plasma-induced defocusing stops further intensity growth. For instance, if we increase the energy of the input pulse from some pre-defined value, the peak intensity in the filament will grow only a little (if at all); nevertheless, the size of the plasma spot and thus the number of free electrons will somewhat increase even if the peak ionization rate remains constant. All this complicated dynamics is absolutely impossible to adequately model with our simple LC model. We can however grasp some key features of this dynamics. And, only if we take them into account, we can achieve plausible explanation of the experimental results.

To start with, let us construct the fields in 2- and 3-color configuration as the Gaussian pulses containing several harmonics as:

$$E_{3\text{col}}(t) = E_0 r_{3\text{col}} (\cos(\omega_p t) + F_{s,3} \cos(\omega_s t + \varphi_{s,3}) + F_{i,3} \cos(\omega_i t + \varphi_{i,3})) e^{-t^2/\tau^2},$$

$$E_{2\text{col}}(t) = E_0 r_{2\text{col}} (\cos(\omega_p t) + F_{s,2} \cos(\omega_s t + \varphi_{s,2})) e^{-t^2/\tau^2}.$$

Here  $E_0$  is the field amplitude; we have taken  $E_0=0.03$  atomic units (intensity around 32 TW/cm<sup>2</sup>) in such a way that the ionization degree remains small for all parameters.  $F_{s,2}$ ,  $F_{s,3}$ ,  $F_{i,3}$  are the dimensionless amplitudes defined as  $F_j = \sqrt{U_j/U_p}$ , where  $U_p$  is the OPA pump  $U_p = 0.55$  mJ,  $U_j$  are the energies of the partial harmonics as defined in Fig. 3 for the 2-color ( $j=\{(s,2), (l,2)\}$ ) and 3-color ( $j=\{(s,3), (l,3)\}$ ) configurations. By such indexing we made clear which parameters are common for both configurations and which can be different.  $\omega_p$ ,  $\omega_i$ ,  $\omega_s$  are the frequencies of the pump, idler and signal waves ( $\omega_p$  corresponds to 790 nm wavelength) and  $\varphi_{s,2}$  and  $\varphi_{i,3}$ ,  $\varphi_{s,3}$  are the corresponding phases (also assumed to be different for 2- and 3-color configurations). For simplicity in our calculations we assume the pulse durations of all partial amplitudes equal to each other, since the result depends only marginally on the pulse duration unless it approaches a single cycle and the ionization degree is small. Here we take FWHM duration  $\tau = 40$  fs. The coefficients  $r_{2\text{col}}$ ,  $r_{3\text{col}}$  are factors which model, in our simple theory, the effects of intensity clamping.

If the pulse propagation effects are neglected,  $r_{2\text{col}}=r_{3\text{col}}=1$ . For an exemplary signal wavelength  $\lambda_s=1480$  nm (which delivers highest THz yield for 3-color configuration as it is seen in Fig. 3) and phases/amplitudes  $\varphi_{s,3} = \frac{\pi}{4}$ ,  $F_{s,3} = 1.314$ ,  $\varphi_{i,3} = \frac{\pi}{8}$ ,  $F_{i,3} = 1.381$  the ionization degree after the pulse  $\frac{\rho}{\rho_0} \approx 0.66$ . Here, the amplitudes are obtained from Fig.3 for  $\lambda_s=1480$  nm and phases are taken to deliver the highest or close to highest THz yield for such configuration; note that in contrast to  $\omega-2\omega$  pulses it is probably not possible to estimate the phases analytically, so we determined them from direct numerical simulation. For the 2-color configuration at the same signal wavelength (which implies  $F_{s,2} = 1.176$  from Fig.3) and the optimal phase  $\varphi_{s,2} = \frac{\pi}{4}$ , the ionization degree after the pulse is significantly lower than in the 3-color case,  $\frac{\rho}{\rho_0} = 0.01$ . The ratio of the THz yields for 3-color  $U_{3\text{col}}$  and 2-color  $U_{2\text{col}}$  configurations calculated from the LC theory under these circumstances, assuming the THz cutoff at 25 THz is  $\frac{U_{3\text{col}}}{U_{2\text{col}}} \approx 5 \times 10^4$ . This is in line with the semi-analytical theory presented below (see Eqs.1-3 below), since from it it follows that  $U_{\text{THz}} \sim \rho^2$ . However, in experiment on Fig. 3 we observe only  $\frac{U_{3\text{col}}}{U_{2\text{col}}} \approx 20$  – much less than the value obtained above.

We attribute this huge discrepancy to the deciding influence of the intensity clamping. To approach the clamping with our simple model, we take  $r_{3\text{col}} < 1$ , that is, we assume that the amplitude of the 3-color pulse is effectively reduced due to defocusing, in such a way that the maximal ionization remains the same as for the 2-color case (in the present case 0.01). Since we are interested only in the ratio  $\frac{U_{3\text{col}}}{U_{2\text{col}}}$  we keep  $r_{2\text{col}}=1$  for simplicity. Under these circumstances we obtain  $r_{3\text{col}}=0.637$ .

Furthermore, we use the following procedure to produce the wavelength scan analogous to the one presented in Fig.3: we first select an optimal signal wavelength  $\lambda_s=1480$  nm for which we determine the optimal phases (given above) for the best THz yield. Then we set  $r_{3\text{col}}=0.637$  which makes, in the

3-color case,  $\frac{\rho}{\rho_0} = 0.01$ , the same as for 2-color one. After that, we scan the signal wavelength keeping  $r_{3\text{col}}$  fixed, and calculate the THz yield for 2-color and 3-color cases from the LC model. Frequency independence of  $r_{3\text{col}}$  should model, though in a somewhat oversimplified form, the modification of the overall free electron number in a filament as we scan the frequency. Note that introducing  $r_{3\text{col}} < 1$  is equivalent to rescaling the input energy  $U_{f,3} = U_p + U_{s,3} + U_{i,3}$  for the 3-color case. Such “rescaled” energy is shown in Fig. 6a in dependence on signal wavelength (red dashed line), together with the “original” input energies for the 3-color and 2-color cases,  $U_{f,2} = U_p + U_{s,2}$  (solid red and black lines, respectively).

The wavelength dependencies of the THz yield for 3-color  $U_{3\text{col}}$  and 2-color  $U_{2\text{col}}$  cases resulting from such procedure are shown in Fig. 6b for the phases of the harmonics being frequency-independent (and given above). For both the 3-color and 2-color cases the shapes of the curves are in agreement with the experiment (see Fig. 3). The ratio of THz yields in 3- and 2-color cases is now around 6, which is somewhat smaller than that obtained experimentally but at least are of the same order of magnitude. The overall decrease of the THz yield as the signal approaches the limiting values of 1600 nm or 1200 nm is the consequence of decrease of the OPA efficiency. For the two color case, the decrease of the THz yield at short wavelength is explained by the fact that the maximum of the THz spectrum moves beyond the cutoff frequency (25 THz).

Furthermore, we were able to reproduce  $\frac{U_{3\text{col}}}{U_{2\text{col}}} \approx 20$  from experiment (Fig. 3), by increasing  $r_{3\text{col}}$  by just around 5% to  $r_{3\text{col}}=0.667$  (see also the “rescaled” pump energy in Fig. 6a shown by blue dot-dashed curve). The corresponding THz yields are plotted in Fig. 6c. For this case the ionization degree for 3-color pulse is  $\frac{\rho}{\rho_0} \approx 0.018$  at  $\lambda_s=1480$  nm, that is, around 2 times more than for the 2-color configuration. This additional increase of  $r_{3\text{col}}$  needed to reproduce experimental results indicate that the number of free electrons in the experiment indeed somewhat increased in the 3-color filament as compared to the 2-color one.

Furthermore, we address the dependence of the THz yield on the phases of harmonics. The curves discussed before were calculated for the phases which are optimal or very close to optimal for  $\lambda_s=1480$  nm. Nevertheless, because our frequencies are anharmonic, the concrete values of phases  $\varphi_{s,2}$  and  $\varphi_{i,3}, \varphi_{s,3}$  play not too much role since the instant phases change with time. This is illustrated in Fig. 6c (dashed lines) where the THz yields for several exemplary phases are plotted. One can see that the yield varies mildly, not more than by factor of 2. Besides, in a spatially extended filament (both 3-color and 2-color) we should see predominantly the THz radiation produced in the areas where the generation efficiency is maximal.

The higher total generation efficiency in the 3-color scheme (even in the case of the same number of free electrons) can be well explained by a semi-analytical theory presented below.

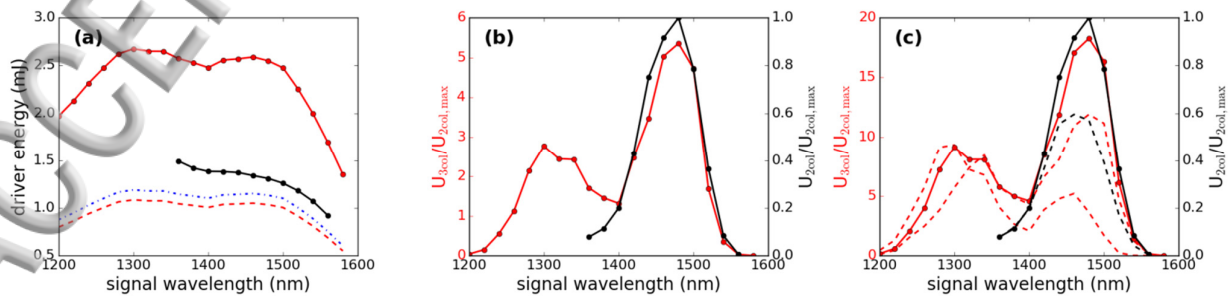


Fig. 6 LC simulations of the THz generation in dependence on the signal wavelength. (a) The overall energies of the driver pulse for 2-color (black solid line) as well for 3-color (red solid line) as given by Fig. 3. Red dashed and blue dash-dotted lines show the “rescaled” driver energies for the 3-color configuration according to intensity clamping argument. They correspond to  $r_{3\text{col}}=0.637$  and  $r_{3\text{col}}=0.667$  and were used to calculate (b) and (c) respectively. (b) THz yield from LC model for the 3-color case (red curve) and 2-color case (black one). The

driver peak intensity for 3-color case (given by red dashed curve in (a)) was rescaled by a constant such that at  $\lambda_s=1480$  nm the ionization after the pulse is the same as for the 2-color configuration. (c) Solid curves show the same as in (b) but with slightly different scaling coefficients [blue dash-dotted line in (a)] so that the result corresponds roughly to the result of experiment. Dashed lines show examples for different phase combinations in the idler and signal (see text for details).

Few representative examples of THz pulse spectra and temporal shapes for different detunings calculated using LC model for 1500 nm signal wavelength and for driver pulse durations of 55 fs (green line) as well as for 100 fs (blue line) are shown in Fig. 7. In the case of three color pump for 55 fs signal duration the spectrum is qualitatively similar to the experimental one presented in Fig. 4a. The wave shapes also demonstrate certain similarity. However, the experimental spectrum in Fig. 4a has an additional 3-lobbed structure which is not reproduced if the pulse with 55 fs is used in calculations, but which appear, with the maxima taking place at roughly the same positions as in the experiment, if the signal pulse duration is taken to be 100 fs. This might be an indication of the propagation-related reshaping of the pump pulses due to dispersion and nonlinear effects during the pulse propagation. For comparison, we also show the spectrum and waveshape obtained using LC theory from the common generation scheme with 800 and 400 nm pumps.

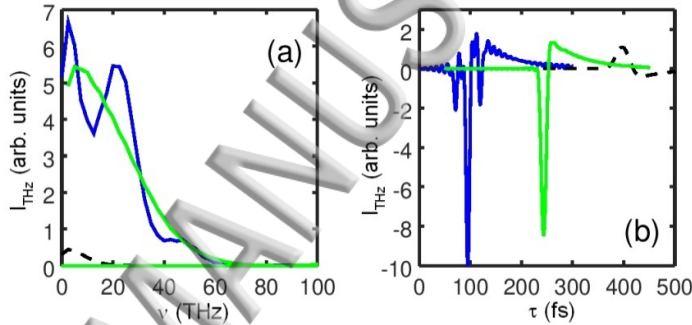


Fig. 7. Spectra (a) and pulse shapes (b) of THz pulses calculated according to the LC model for the three-color pump configuration (solid lines) assuming the signal wavelength of 1500 nm, pulse duration of 55 fs (green line) and of 100 fs (blue line). For comparison, the output of a common two-color scheme (with two pump waves of wavelengths 800 and 400 nm) is given by the black dashed lines (for visibility, these curves are multiplied by 10 times in (a) and 4 times in (b)).

One can see that the 3-color pump produces much broader signal in comparison with the 2-color one.

Both increase of the overall efficiency and broader spectrum can be well explained using a diffraction-grating analogy developed in [20,26]. According to this approach the electrons are ionized close to the maxima of the driver electric field, thus forming a set of “ionization events”  $t_n$ . The plasma-induced current produced by the electrons ionized at the time  $t_n$ , in turn, is approximately given by

$$J(t) = e\delta\rho(t_n)(A(t) - A(t_n)), \quad (1)$$

where  $e$  is the electron charge,  $\delta\rho(t_n)$  is the electron number produced at  $t_n$ , and  $A(t)$  is the vector potential of the driving field  $A(t) = \int_{-\infty}^t E(\tau)d\tau$ . Using Eq.(1), the resulting THz radiation can be represented as a sum of contributions from every wave:

$$E_{\text{THz}} \sim \sum_n S(n, \omega), \quad (2)$$

Where  $S(n, \omega)$  is the “strength” of every ionization event defined by

$$S(n, \omega) = \delta\rho(t_n)A(t_n)\exp(i\omega t_n). \quad (3)$$

For the lowest frequencies in THz range ( $\omega \approx 0$ ) we have  $S(n, 0) = \delta\rho(t_n)A(t_n)$ . This equation has simple interpretation: since the velocity of the electron at  $t \rightarrow \infty$ , which was born at the time  $t_n$  is

proportional to  $A(t_n)$ , this equation says us that the THz field is proportional to the number of electrons times velocity of electron at infinity.  $S(n, 0)$  are shown for few exemplary waveforms in Fig. 8 as blue bars, together with corresponding waveshape (red line). The values of  $A(t_n)$  are intrinsically limited by the type of waveform used in experiment. Note that  $t_n$  are determined by the condition  $|E(t_n)|=\text{max}$ . Thus, for instance, for the case of 1-color pulse  $A(t_n)$  is very close to zero because, if our field shape is proportional to  $\cos(\omega t)$ , then  $t_n=\pi n$ , and  $A(t_n)\sim\sin(\omega t_n)\approx 0$  (the small deviation is due to the slow field envelope). For 2-color fields, one can make these values deviate from zero. 3-color fields provide even more degrees of freedom to improve  $A(t_n)$ . The ideal waveshape (taking into account intensity clamping) should contain many frequencies and looks like a saw-tooth shape [26], and, formally speaking, a 3-color pump can better approach this ideal waveshape than in a 2-color case. In our case however, we have 3-color anharmonic pulses, thus the THz yield is less than obtainable with a 3-color saw-tooth approximation. This is especially true if we take into account intensity clamping as we did above. Nevertheless, as it was also shown above, even such „nonoptimal” 3-color waveforms can significantly increase the THz radiation yield.

Furthermore, the simple LC theory allows also to explain the spectral broadening of the pulses in 3-color case as compared with 2-color one. Namely, Eqs. 1,2 define a linear “grating” in frequency domain, with ionization events at the times  $t_n$  playing a role of “point-like emitters”. The radiation from a single emitter is very broadband, and the narrow maxima in frequency space appear as a result of interference in frequency space of these broadband contributions. The THz radiation is a 0<sup>th</sup> order diffraction maximum in this representation. The width of the maximum is defined by the number of “emitters” (that is, by the number of ionization events) and by the periodicity of their arrangement. Thus the common 2-color (harmonic) scheme defines a much more periodic grating than the 3-color one (see Fig. 8), and thus the more narrow maximum in the frequency space. That is, aperiodicity of ionization events in 3-color case is the reason for the broader spectrum.

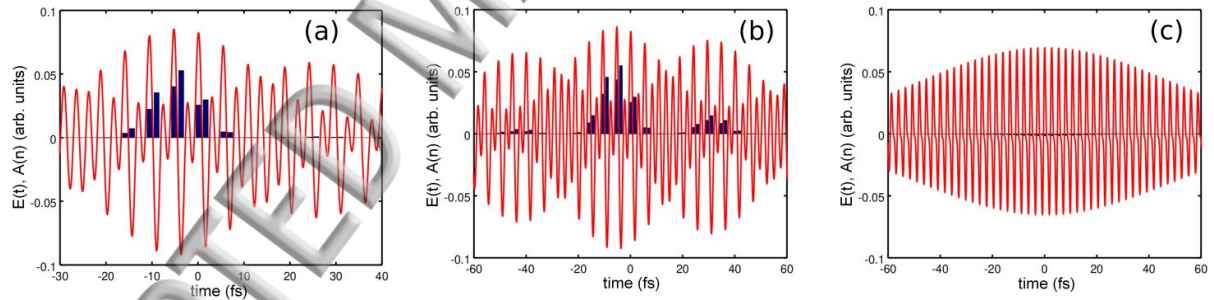


Fig. 8. Driver field waveforms  $E(t)$  (red lines) and strengths of ionization events  $S(n, 0)$  for the ionization events (blue bars) according to the LC model for 3-color configuration corresponding to the parameters of Fig. 7, with pulse duration of 55 fs (a) and 100 fs (b). In (c) the common two-color scheme (with two pump wavelengths of 800 and 400 nm) is represented with the  $S(n, 0)$  multiplied by factor of 6 for visibility.

Note that in the LC model, the pump propagation effects can not be taken into account. More advanced model [15,16,20,22] would include nonlinear effects of the propagating pump as well as interference of THz contributions from the different spatial positions. Both these effects can significantly modify THz radiation (even beyond the clamping effects discussed above). Also, the spectral shape of the THz wave is modified significantly upon the propagation of THz radiation to the observer. All these effects are expected to be especially important in the case of filaments (in contrast to plasma spots). The LC model also can not provide the absolute values of THz conversion efficiencies – one can only compare the efficiencies for 2- and 3-color cases. Nevertheless, quite surprisingly, as one can see, even such simple theory grasps most of the features of generated THz radiation in our experiment.

## 5. Conclusions

We have investigated the energy, spectral and spatial properties of terahertz radiation, generated in air by focused femtosecond three- and two-color laser pulses. It was found that in the case of three-color pump the overall terahertz generation efficiency in filament can reach up to  $10^{-5}$ . The spectrum of THz radiation, generated by the three-color pump pulses, was found to be a broadband one, extending at least up to 50 THz, while the two-color THz emission consists mainly of a single spectral band centered at about 8 THz. In both cases the THz beam had a conical shape with the apex angle of about 5 degrees, which in general is consistent with previous studies. The results are in qualitative agreement with the theoretical predictions based on THz frequency generation via ionization-induced nonlinearity (Brunel harmonics). If compared to the typical plasma spot experiments, our efficiency is around one order of magnitude smaller. We attribute this to the low free electron density in a filament. On the other hand, as the results of the present article show, if we compare the 2- and 3-color experiments in a similar filamentary configuration, the 3-color case has a clear advantage in energy by about one order of magnitude.

Our simple theoretical consideration provides arguments that three main players can be identified: i) In a 3-color anharmonic waveshapes, at certain temporal points the fields from all the sub-pulses summs up constructively, producing strong peak field and leading to much stronger ionization. ii) On the other hand, due to the intensity clamping, the peak intensity in a filament does not increase or increase only marginally in comparision to the 2-color case. iii) Nevertheless, even if the same number of free electrons are produced, the 3-color waveshapes are still capable to produce faster electrons, which on its own may increase THz yield several times.

Comparision of our simplified theory with the experimental results indicates that in our 3-color filaments both the speed of electrons at  $t \rightarrow \infty$  and number of free electrons increases in comparision to the 2-color case. These both mechanisms participate approximately equally in the resulting THz yield increase (that is, ~5 times due to increase of electron speeds and ~5 times due to increase of the electron number). Nevertheless, our analysis must be considerd as only preliminary since many effects such as spatio-temporal reshaping of the pump pulses were not considered here at all. Significant broadening of the spectrum in the 3-color case in comparison to the harmonic 2-color one can be explained by an aperiodicity of the ionization events in time. In this “diffraction grating” picture [20], the THz radiation is the 0<sup>th</sup> order diffraction order generated by responses from different ionization events. The spectral broadening arises because the sequence of ionization events is not anymore periodic and thus resembles an aperiodic diffractive grating.

## Acknowledgment

The research leading to these results has received funding from LASERLAB-EUROPE (grant agreement no. 654148, European Union’s Horizon 2020 research and innovation programme), I.B. and U.M thank to Deutsche Forschungsgemeinschaft (DFG), projects (BA 4156/4-2, MO 850-19/2) as well as Germany’s Excellence Strategy within the Cluster of Excellence PhoenixD (EXC 2122, Project ID 390833453).

## References

1. D. J. Cook and R. M. Hochstrasser, Opt. Lett. **25**, 1210–1212 (2000).
2. M. D. Thomson, M. Kress, T. Loffler, and H. Roskos, Laser Photonics Rev. **1**, 349–368 (2007).
3. B. Clough, J. Dai, and X.-C. Zhang, Mater. Today **15**, 50–58 (2012).
4. K. Y. Kim, A. J. Taylor, J. H. Glownia, and G. Rodriguez, Nat. Photonics **2**, 605–609 (2008).
5. I. Oh, Y. S. You, N. Jhajj, E. W. Rosenthal, H. M. Milchberg and K. Y. Kim, New Journal of Physics **15**, 075002 (2013).

6. Y.-J. Yoo, D. Kuk, Z. Zhong, and K.-Y. Kim, IEEE J. Sel. Topics Quantum Electron. **23**, 8501007 (2017).
7. Y. Minami, T. Kurihara, K. Yamaguchi, M. Nakajima, and T. Suemoto, Appl. Phys. Lett. **102**, 041105 (2013).
8. J. Dai, X. Xie, and X.-C. Zhang, Phys. Rev. Lett. **97**, 103903 (2006).
9. N. Karpowicz, J. Dai, X. Lu, Y. Chen, M. Yamaguchi, H. Zhao, X.-C. Zhang, L. Zhang, C. Zhang, M. Price-Gallagher, C. Fletcher, O. Mamer, A. Lesimple, and K. Johnson, Appl. Phys. Lett. **92**, 011131 (2008).
10. J. Liu and X.-C. Zhang, Phys. Rev. Lett. **103**, 235002 (2009).
11. B. Clough, J. Liu and X.-C. Zhang, Opt. Lett. **36**, 2399-2401 (2011).
12. I-Chen Ho, Xiaoyu Guo, X.-C. Zhang, Opt. Express **18**, 2872-2883 (2010).
13. A. Nahata and T. F. Heinz, Opt. Lett. **23**, 67–69 (1998).
14. W.-M. Wang, S. Kawata, Z.-M. Sheng, Y.-T. Li, L.-M. Chen, L.-J. Qian, and J. Zhang, Opt. Lett. **36**, 2608-2610 (2011).
15. L. Bergé, S. Skupin, C. Köhler, I. Babushkin, J. Herrmann, Phys. Rev. Lett. **110**, 073901 (2013).
16. A. Nguyen, P.G. de Alaiza Martínez, J. Déchard, I. Thiele, I. Babushkin, S. Skupin, L. Bergé, "Opt. Express **25**, 4720 (2017).
17. M. Clerici, M. Peccianti, B. E. Schmidt, L. Caspani, M. Shalaby, M. Giguére, A. Lotti, A. Couairon, F. Légaré, T. Ozaki, D. Faccio, and R. Morandotti, Phys. Rev. Lett. **110**, 253901 (2013).
18. N. V. Vvedenskii, A. I. Korytin, V. A. Kostin, A. A. Murzanev, A. A. Silaev, and A. N. Stepanov, Phys. Rev. Lett. **112**, 055004 (2014).
19. M. D. Thomson, V. Blank, and H. G. Roskos, Opt. Express, **18**, 23173-23182 (2010).
20. I. Babushkin, S. Skupin, A. Husakou, C. Koehler, E. Cabrera-Granado, L. Bergé, J. Herrmann, New J. Phys. **13**, 123029 (2011).
21. I. Babushkin, C. Brée, C. M. Dietrich, A. Demircan, U. Morgner, A. Husakou, J. Mod. Opt. **64**, 1078 (2017).
22. T. Balčiūnas, D. Lorenc, M. Ivanov, O. Smirnova, A. M. Zheltikov, D. Dietze, K. Unterrainer, T. Rathje, G. G. Paulus, A. Baltuška and S. Haessler, Opt. Express, **23**, 15278-15289 (2015).
23. L.-L. Zhang, W.-M. Wang, T. Wu, R. Zhang, S-J Zhang, C.-L. Zhang, Y. Zhang, Z.-M. Sheng, and X-C. Zhang, Phys. Rev. Lett. **119**, 235001 (2017).
24. V. A. Kostin, I. D. Laryushin, A. A. Silaev, and N. V. Vvedenskii. Phys. Rev. Lett., **117**, 035003 (2016).
25. W.-M. Wang, Z.-M. Sheng, Y.-T. Li, Y. Zhang, and J. Zhang, Phys. Rev. A **96**, 023844 (2017).
26. P. González de Alaiza Martínez, I. Babushkin, L. Bergé, S. Skupin, E. Cabrera-Granado, C. Köhler, U. Morgner, A. Husakou, and J. Herrmann, Phys. Rev. Lett. **114**, 183901 (2015).
27. J. D. Bagley, C. D. Moss, S. A. Sorenson, and J. A. Johnson, J. Phys. B: Atom., Molecul. Opt. Phys. **51**, 144004 (2018).
28. V. A. Andreeva, O. G. Kosareva, N. A. Panov, D. E. Shipilo, P. M. Solyankin, M. N. Esaulkov, P. González de Alaiza Martínez, A. P. Shkurinov, V. A. Makarov, L. Bergé, and S. L. Chin Phys. Rev. Lett. **116**, 063902 (2016).
29. T.-J. Wang, Y. Chen, C. Marceau, F. Théberge, M. Châteauneuf, J. Dubois, and S. L. Chin, Appl. Phys. Lett. **95**, 131108 (2009).
30. T.-J. Wang, S. Yuan, Y. Chen, J.-F. Daigle, C. Marceau, F. Théberge, M. Châteauneuf, J. Dubois, and S. L. Chin, Appl. Phys. Lett. **97**, 111108 (2010).
31. E. J. Galvez, P. M. Koch, JOSA A **14**, 3410–3414 (1997).
32. N. S. Makarov, M. Drobizhev, and A. Rebane, Opt. Express **16**, 4029-4047 (2008).
33. H. Zhao, L. Zhang, S. Huang, S. Zhang, and C. Zhang, IEEE THz Sc. Techn. **8**, 299 (2018).
34. V. Vaičaitis, M. Kretschmar, R. Butkus, R. Grigonis, U. Morgner, I. Babushkin, J. Phys. B: At. Mol. Opt. Phys. **51**, 045402 (2018).

35. X. -L. Liu, X. Lu, X. Liu, L.-B. Feng, J.-L. Ma, Y.-T. Li, L.-M. Chen, Q.-L Dong, W. -M. Wang, Z. -H. Wang, Z. -Y. Wei, Z. -M. Sheng, J. Zhang, Opt. Lett. **36**, 3900-3903 (2011).
36. E. Gaižauskas, V. Vaičaitis, O. Fedotova, and O. Khasanov, Opt. Mat. Express, **5**, 623-628 (2015).
37. E. Gaižauskas, D. Pentaris, T. Efthimiopoulos, and V. Vaičaitis, Optics. Lett. **38**, 124-126 (2013).
38. V. Pyragaite, V. Smilgevičius, K. Steponkevičius, B. Makauskas, and V. Vaičaitis, JOSA B **31**, 1430–1435 (2014).
39. V. Blank, M. D. Thomson and H. G. Roskos, New J. Phys., **15**, 075023 (2013).
40. V. Vaičaitis, M. Ivanov, K. Adomavičius, Ž. Svirskas, U. Morgner, I. Babushkin, Laser physics **28**, 095402 (2018).
41. Y. S. You, T. I. Oh, and K. Y. Kim, Phys. Rev. Lett. **109**, 183902 (2012).
42. A. Gorodetsky, A. D. Koulouklidis, M. Massaouti, and S. Tzortzakis, Phys. Rev. A **89**, 033838 (2014).
43. L. W. Keldysh, Sov. Phys. JETP **20** 1307- 1314 (1965).

ACCEPTED MANUSCRIPT

